

Spherical Conformal Bow-Tie Antenna for Ultra-Wide Band Microwave Imaging of Breast Cancer Tumor

İ. Ünal¹, B. Türetken^{1,2}, and C. Canbay³

¹ Millimeter Wave and Terahertz Technologies Research Laboratories (MILTAL)
Material Institute, TUBITAK-MRC, Gebze, Kocaeli, 41470, Turkey
ilhami.unal@tubitak.gov.tr, bahattin.turetken@tubitak.gov.tr

² TUBITAK-BILGEM, Gebze, Kocaeli, 41470, Turkey

³ Department of Electrical and Electronics Engineering
Yeditepe University, İstanbul, 34755, Turkey
canbay@yeditepe.edu.tr

Abstract — In this paper, contribution of spherical conformal ultra-wide band (UWB) bow-tie antenna on enhancement of breast tumor detection capability of a radar-based microwave imaging system is investigated through simulation, demonstrating the potential of the novel antenna element used in a half-spherical antenna array surrounding the breast. The designed conformal antenna operates efficiently across the band from 1 GHz to 8 GHz, and it is immersed in a coupling medium in order to get a good impedance matching with the breast. Images are successfully formed by using delay-and-sum (DAS) algorithm for the detection of a spherical tumor model with 2 mm diameter. The tumor is located at 40 mm depth inside three different breast phantom models with homogeneous fatty breast tissue, quasi-heterogeneous mix of fibro-glandular and fatty breast tissues and homogeneous fibro-glandular tissue, respectively. Fidelity factor, indicating the maximum cross correlation between observed and excitation pulses, of the conformal bow-tie is found to be around 13% more than that of the planar bow-tie at 40 mm depth. The use of the spherical conformal antenna presents an excellent solution to increase tumor responses by at least 2.3 dB, as well as to decrease mutual coupling effects between array elements, compared to the same system with planar bow-tie antennas.

Index Terms - Breast cancer, conformal bow-tie antennas, and UWB microwave imaging.

I. INTRODUCTION

Early diagnosis and treatment are the hot keys to survive from breast cancer. The present “golden” standard screening technology for detecting early-stage breast cancer is X-ray mammography. However, it has several limitations, especially when dealing with younger women who have dense breast tissues. It also requires painful and uncomfortable breast compression and exposes the patient to ionizing radiation.

Electromagnetic waves and antennas have a huge application area, and one of the challenging areas is remote sensing systems and detection systems using microwaves, today. Increasing demand on non-destructive sensing or detecting breast tumor keeps this subject hot in this field. There are various passive and active microwave techniques, which have been proposed as an alternative especially to the most widely used X-ray mammography; such as microwave radiometry [1], hybrid microwave-induced acoustic imaging [2], microwave tomography [3], and UWB microwave radar technique [4-6].

Currently, there are two main active methods that involve illuminating the breast with microwaves and then measuring transmitted or backscattered signals, such as microwave

tomography and radar-based imaging. In microwave tomography, a nonlinear inverse scattering problem is solved to reconstruct an image of the spatial distribution of dielectric properties in the breast. On the other hand, UWB radar-based imaging approach deals with only to identify the presence and location of significant scattering obstacles such as malignant breast tumors [7].

There is a small contrast between healthy and diseased breast tissues at X-ray frequencies [4]. However, resolution in X-rays is absolutely better than in microwaves. On the other hand, the physical basis for microwave detection of breast tumor is the significant contrast in the electrical properties of the normal and the malignant breast tissues [4], which exists in the earliest stage of tumor development. Another advantage of the microwave imaging technique is that it would be nonionizing and it doesn't require painful breast compression. Other available screening techniques such as ultrasound and MRI are either less effective or are too costly.

Because of its excellent advantages, recent years have shown a dominant interest in UWB microwave imaging technique, for a particular technique to detect and locate a breast tumor [4-15]. This technique specifically involves transmitting and receiving short duration pulses for various locations of UWB probe antenna or alternatively by an antenna array controlled with switches. The UWB imaging technique offers creation of an image, which can be formed by combining all of the signals (S_{ii} and S_{ij} , $i \neq j$) coming from different antennas. Well-known DAS algorithm would be used to create microwave images of breast cancer tumors [4]. In order to enhance tumor detection capability, the radar-based technique requires the use of more sensitive antennas operating over a considerable UWB frequency range.

In this study, UWB microwave imaging technique is used in the 1 GHz – 8 GHz frequency range, which guarantees balance between reasonable contradictory needs of better spatial resolution, better penetration depth [11], less attenuation of electromagnetic waves through the breast and smaller dimensions of a multi-function active imaging system. The selected frequency range is expected to provide reasonable tumor detection capabilities. In particular, since the skin

reflections back to the antenna adversely affect imaging results, better penetration of electromagnetic waves into the breast tissue will be determined by operating the antenna in a coupling medium whose dielectric properties are close to the breast tissue. Antenna size would also be selected to be smaller since the wavelength in the coupling medium will be smaller than air.

Several different types of antennas have been considered and reported over the past decade by research groups involved in radar-based UWB breast imaging; such as ridged pyramidal horn [7], UWB planar bow-tie [8], cross-polarized types [9-10], U-slot [11-12], antipodal Vivaldi [13], stacked microstrip patch [12, 14], tapered slot [15], etc. These antennas were generally used and tested in planar, cylindrical or spherical scanning surfaces, as a single element or in an antenna array. There are also a lot of advantages of using circular or hemispherical antenna array configurations compared to planar ones; such as increased tumor detection sensitivity, enhancement on signal reception [16], increased illuminated coverage area inside the breast [17], better signal-to-clutter (S/C) ratio [18], etc. However, mutual coupling effects of array elements can negatively impact antenna performance and imaging results, too [19].

On the other hand, in order to detect the weak reflections from small tumors located in tissues ranging from fatty breast to glandular, a high sensitive antenna is required to send and receive electromagnetic waves with low pulse distortion and low mutual coupling effects in the array. Since antennas are assumed to be operating in the near field region in which spherical waves exist, antenna geometry and polarization should be appropriately selected to perfectly match with the spherical waves inside the breast, too [20].

This paper presents herein spherical conformal bow-tie antennas to improve tumor detection capability of the microwave imaging system. Conventional planar UWB bow-tie antennas are curved onto a hemi-sphere surface to investigate its effects on enhancement of tumor responses and signal energies [21].

Seven UWB spherical conformal bow-tie antennas are located 4.7 mm above different half-spherical breast phantoms that are modeled on the full-wave electromagnetic simulator (CST Microwave Studio®), which is based on the FIT

method, to calculate the performance of the antennas. All of the time-domain signals (S_{ii} and S_{ij} , $i \neq j$) coming from different antennas are obtained from the simulation model with and without 2 mm diameter tumor at 40 mm depth inside breast phantom models with homogeneous fatty breast tissue, quasi-heterogeneous mix of fibro-glandular and fatty breast tissues, and homogeneous fibro-glandular tissue, by feeding each antenna sequentially. Recorded data are processed on DAS algorithm, and then images of the computed backscattered signal energies for each pixel are created as a function of position. Imaging results of the microwave imaging system with the conformal bow-tie antennas are successfully compared to the same system with planar bow-tie antennas.

This paper is organized as follows: the layered half-spherical breast phantom model, antenna design results and antenna array structure are introduced with comparative antenna simulations in section 2, followed by pulse distortion analysis. In section 3, after briefly outlining the DAS imaging algorithm, imaging results and discussions are given for different breast phantom models. Section 3 also presents tumor responses for the novel antenna and mutual coupling effects of array elements with comparative results in details. Finally, the findings of the study are briefly given in section 4.

II. SIMULATION STUDY

A. Layered half-spherical breast phantom models

Layered breast phantom model consists of a skin tissue layer with thickness of 2 mm and three different half-spherical tissues with radius of 58 mm under the skin, such as homogeneous fatty breast, quasi-heterogeneous mix of fibro-glandular

and fatty breast, and homogeneous fibro-glandular tissues (Fig. 1). The homogeneous fatty breast, quasi-heterogeneous and homogeneous fibro-glandular phantom models represent “mostly fatty”, “heterogeneously dense” and “very dense” phantom models, respectively.

The breast phantom is surrounded by a coupling medium in which antennas are placed, to reduce adverse effects of signal reflections at the antenna-air-breast interface [15]. Non-dispersive relative dielectric permittivity ϵ_r and conductivity σ values of skin, ducts, fatty breast, fibro-glandular and tumor tissues are selected, as in Table I. Dielectric properties of the coupling medium are selected as $\epsilon_r = 9$, $\sigma = 0$ S/m [18].

Table I: Dielectric properties of the tissues.

Tissue	ϵ_r	σ (S/m)
Skin [15]	36	4
Ducts [11]	37.96	4.5
Fatty Breast Tissue [7]	9	0.4
Glandular Tissue [11]	21.5	1.7
Tumor [18]	50	7

Differently sized glands of spherical (radius 8.5 mm $< r < 12.5$ mm) shape [22] are embedded in the fatty breast tissue for the quasi-heterogeneous phantom model, as shown in Fig. 1 (b).

B. Antenna design

Use of the spherical conformal antenna structure is presented here for breast cancer imaging, and it is aimed to be used as an element of a microwave imaging system operating between 1 GHz and 8 GHz. The intended use of conformal antenna is expected to increase the dynamic range of the system as well as to diminish mutual

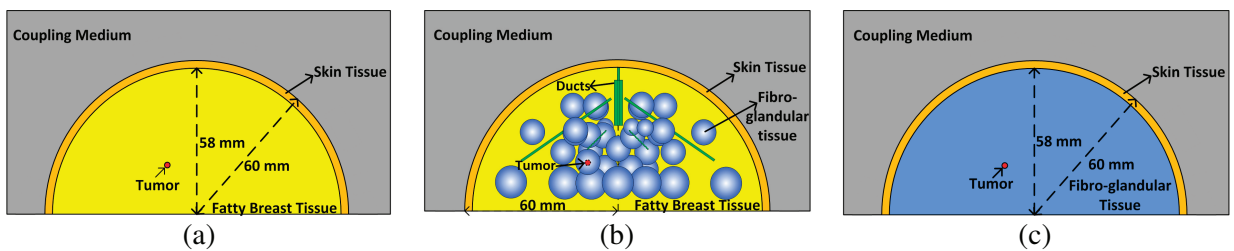


Fig. 1. Schematic illustration of layered half-spherical breast phantom models with (a) homogeneous fatty breast tissue, (b) quasi-heterogeneous mix of fibro-glandular and fatty breast tissues, and (c) homogeneous fibro-glandular tissue.

coupling effects between array elements and pulse signal distortion through the breast.

The planar bow-tie antenna (26 mm × 40 mm), which is curved onto a hemi-sphere surface is aimed to be used as an UWB probe element of a half-spherical antenna array (Fig. 2 (a)). The wavelength at the center frequency (4.5 GHz) is 22 mm inside the coupling medium. The antenna-skin distance has been obtained as 4.7 mm, by optimizing the distance with parametric sweep for the purpose of best matching over the bandwidth. This value is close to the expected theoretical distance, which is approximately quarter-wavelength at the center frequency [23, 24]. If the antennas are not located at this optimal distance, the antenna gain is reduced.

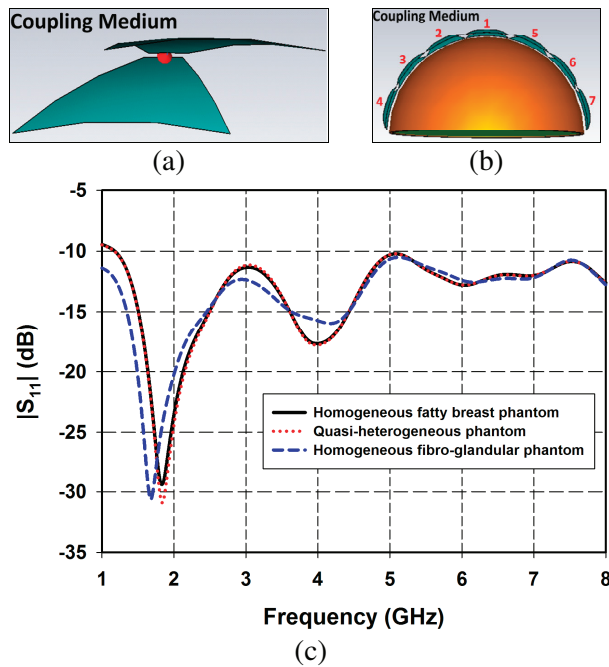


Fig. 2. (a) Spherical conformal bow-tie antenna, (b) simulation model of spherical conformal bow-tie antenna array in front of the breast phantom, and (c) return loss of the spherical conformal bow-tie antenna in the half-spherical antenna array encircling different breast phantoms.

The conformal bow-tie antenna is designed for operating with other antenna elements in the half-spherical antenna array and also in front of the breast phantom model (Fig. 2 (b)). Comparative results of return loss of the conformal bow-tie antenna encircling different breast phantom models

are shown in (Fig. 2 (c)). The simulation results are obtained for the 1st antenna located at the center of the half-spherical antenna array, as shown in Fig. 2 (b). The results show that the -10 dB bandwidth of the antenna, which is operating in the half-spherical antenna array surrounding the breast phantom extends from nearly 1 GHz to above 8 GHz.

As the UWB microwave imaging system operates in the time domain by sending a narrow pulse to penetrate the breast and measures the scattered pulses, it is important to study distortion when the radiated pulse propagates through especially the quasi-heterogeneous breast phantom [15]. For this purpose, the transmitted pulse from the 1st antenna located at the center of the half-spherical antenna array is monitored at different distances normal from the antenna aperture. The time domain performance of the conformal bow-tie antenna will be compared to that of the planar bow-tie antenna, as in Fig. 3.

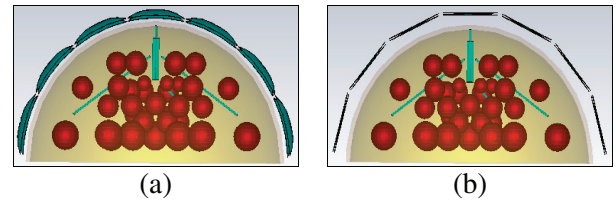


Fig. 3. (a) Spherical conformal bow-tie antennas and (b) planar bow-tie antennas, in the presence of quasi-heterogeneous breast phantom model.

In order to find out the distortion level in the transmitted pulses inside the breast phantom model, the fidelity factor is calculated at different locations within the breast. The fidelity factor is defined as the maximum magnitude of the cross correlation between the observed pulse ($s_R(t)$) at a certain distance and the excitation pulse ($s_T(t)$) [12],

$$F = \max_{\tau^d} \frac{\int_{-\infty}^{\infty} s_T(t) s_R(t - \tau^d) dt}{\sqrt{\int_{-\infty}^{\infty} |s_T(t)|^2 dt \cdot \int_{-\infty}^{\infty} |s_R(t)|^2 dt}}, \quad (1)$$

where τ^d is the required time delay for obtaining maximum magnitude of the cross correlation.

The results indicate an increasing pulse distortion as the signal propagates through the

heterogeneous breast phantom due to the multiple reflections inside the phantom model [15]. For the case with planar bow-tie antenna, the fidelity factor decreases more and it becomes 45.2 % at 40 mm depth inside the breast (Fig. 4). On the other hand, the fidelity factor is kept at higher values in overall when the antenna is spherical conformal bow-tie. That is around 58.2 % at 40 mm depth inside the breast. Moreover, for the conformal bow-tie antenna presented in this paper, the fidelity factor is within reasonable values (around more than 60 %) even inside the breast phantom [25].

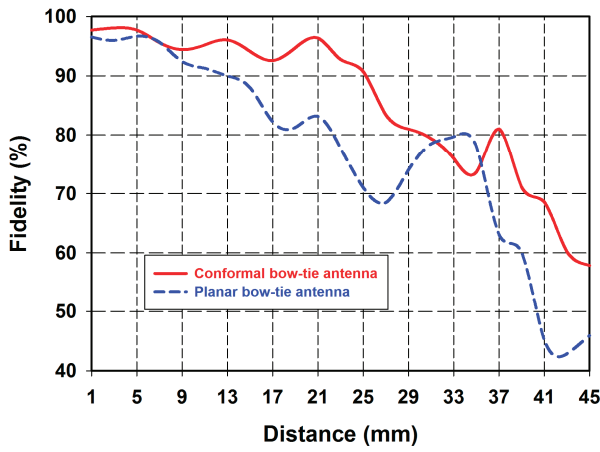


Fig. 4. Calculated fidelity factors with respect to distance from the antenna, in the presence of quasi-heterogeneous breast phantom model.

In order to find out mutual coupling effects of array elements in Fig. 3, conformal and planar bow-tie antennas are compared to each other for S_{21} characteristics between the 1st and 2nd antennas, as shown in Fig. 5. It is observed that the overall S_{21} characteristics of the conformal antenna show less mutual coupling effects, with the exception of higher coupling effects in around 1 GHz - 1.3 GHz and 3.6 GHz - 5 GHz frequency bands. However, these bands correspond to 24 % of the whole band. Moreover, the areas under the curves of S_{21} characteristics versus frequency for the conformal antenna are less than that of the planar antenna, indicating lower mutual coupling effects in the overall.

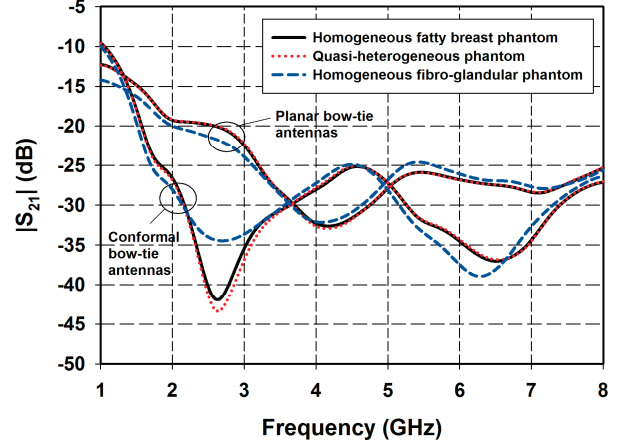


Fig. 5. S_{21} characteristics of conformal and planar bow-tie antennas in the half-spherical antenna array encircling different breast phantoms.

III. IMAGING RESULTS AND DISCUSSION

When one of the seven UWB bow-tie antennas in the array is excited by Gaussian pulse, backscattered time-domain signals (S_{ii} and S_{ij} , $i \neq j$) are recorded. This procedure is repeated by feeding each antenna sequentially, for cases with and without 2 mm diameter tumor. Therefore, 49 time-domain signals (including 28 independent time-domain signals) coming from different antennas are recorded for each case. Tumor response signals S_{ij}^T are obtained by calibrating the recorded signals as in equation (2),

$$S_{ij}^T = S_{ij} \Big|_{\text{with tumor}} - S_{ij} \Big|_{\text{without tumor}}. \quad (2)$$

The tumor response signals are additionally compensated for $1/r$ attenuation of electric fields inside the breast. When the 1st antenna is fed and signal is received from 3rd antenna, one can easily compute time delay for the possible tumor location depicted in Fig. 6. Accordingly, time delay between the transmitted signals from 1st antenna and the received signal by 3rd antenna can be computed as in equation (3), regarding velocities of electromagnetic fields in different media, individually,

$$\tau_{31}^d(\vec{r}) = \frac{d_1^{31}(\vec{r})}{v_{\text{coupling}}} + \frac{d_2^{31}(\vec{r})}{v_{\text{skin}}} + \frac{d_3^{31}(\vec{r})}{v_{\text{breast}}} + \frac{d_4^{31}(\vec{r})}{v_{\text{breast}}} + \frac{d_5^{31}(\vec{r})}{v_{\text{skin}}} + \frac{d_6^{31}(\vec{r})}{v_{\text{coupling}}}. \quad (3)$$

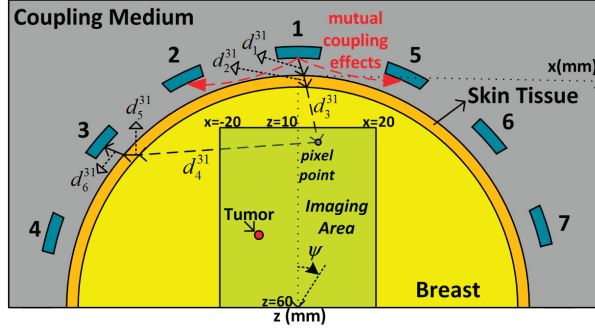


Fig. 6. Illustration of mutual coupling effects (red paths) and signal path, when 1st antenna is fed and 3rd antenna is in receiving mode (black path).

In fact, the heterogeneity of the breast would change the velocities inside the breast. As the antenna positions with respect to each other are known, the mean velocities inside three different breast phantom models are successfully obtained by using time-delay differences between arbitrarily selected S_{54} and S_{74} time-domain signals, as shown in Fig. 7. Although, the DAS algorithm is known as unsuitable for the frequency dispersive tissues, the same practical method can also be successfully used with the DAS algorithm for both heterogeneous and dispersive breast phantom models without any detected tumor location error [21]. However, only non-dispersive case is considered for simplicity, in this paper.

Total tumor response for each pixel is obtained, as in equation (4), regarding computed time delays between each antenna and pixel points, one by one [4]. Then, images of the computed scattered signal energies for each pixel are created as a function of position,

$$T(\vec{r}) = \left[\sum_{i=1}^7 \sum_{j=1}^7 S_{ij}^T(\tau_{ij}^d(\vec{r})) \right]^2 \quad (4)$$

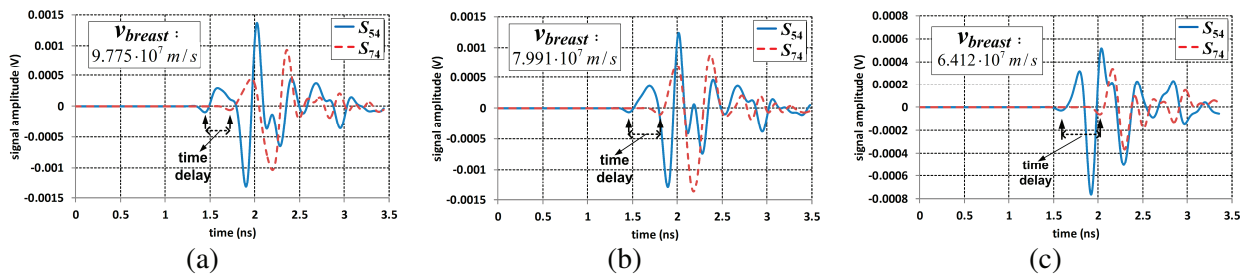


Fig. 7. Velocities obtained by using time delays between S_{54} and S_{74} signals for (a) homogeneous fatty, (b) quasi-heterogeneous, and (c) homogeneous fibro-glandular breast phantom models.

Firstly, the effect of spherical conformal antenna structure on the tumor response will be compared to that of the planar bow-tie antenna. Three different breast phantom models are used in the simulations. Since the peak-to-peak voltage of the excitation pulse ($s_T(t)$) is 1.7 V, the tumor response (in dB) is calculated using the “uncompensated” time-domain tumor response signals S_{ij}^T , as follows [8],

$$Tumor\ Response(dB) = 20 \cdot \log \left(\frac{(S_{ij}^T)_{peak-peak}}{1.7} \right) \quad (5)$$

Tumor responses (in dB) corresponding to highest signal levels S_{12}^T and lowest signal levels S_{17}^T , are given in Fig. 8, with comparable results for conformal and planar bow-tie antennas operating in the presence of different breast phantom models. Each neighbor antenna is separated by 25° with respect to the bottom center of the breast phantom (0, 0, 60 mm). As an example, in the case of S_{42}^T , S_{12}^T , and S_{72}^T tumor response signals, ψ is equal to -75° , 0° , and 75° , respectively (See Fig. 6).

Comparing the calculated tumor response levels of the conformal bow-tie antenna with those of the planar bow-tie antenna, they increase when the conformal antennas are used (Fig. 8). Signal enhancement is observed between 2.3 dB and 5.7 dB in overall for the conformal antenna case. The reduction of tumor responses in the planar bow-tie antenna case is possibly related with worse pulse distortion and mutual coupling effects (Fig. 7). The conformal structure also achieves good polarization matching with spherical waves inside the breast, because of its spherical conformal geometry, too [20]. The tumor response levels of

S_{67}^T and S_{77}^T show unexpected increment for the case of antennas operating in the presence of homogeneous fibro-glandular breast phantom, as shown in Fig. 8 (b). Obtained S_{67}^T and S_{77}^T signals are found to be lower than the minimum detectable signal level in the simulation software, resulting wrong computation of tumor responses.

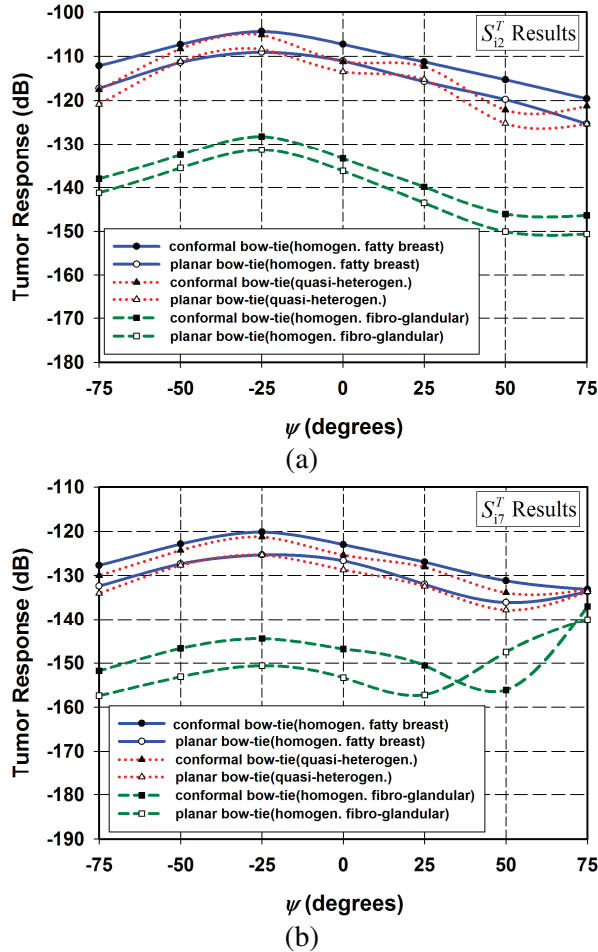


Fig. 8. Results of tumor responses (dB) corresponding to (a) S_{12}^T and (b) S_{17}^T , with respect to ψ .

On the other hand, the peak tumor responses of the conformal antenna for both S_{12}^T or S_{17}^T are found about 1 dB and 23 dB larger when the antenna is operated in the presence of homogeneous fatty breast and quasi-heterogeneous phantoms, respectively, than when it's operated in the presence of homogeneous fibro-glandular breast phantom. The tumor response results, in

Fig. 8, also show dynamic range requirements for the detection of the tumor with 2 mm diameter at 40 mm depth. Since dynamic range of a vector network analyzer can reach down to -140 dB for experimental measurements [26], the tumor responses are not high enough to detect the tumor embedded in the homogeneous fibro-glandular breast, mimicking very dense breast tissue.

Moreover, the area under the curves of tumor responses versus different ψ angles decreases as the breast becomes denser with fibro-glandular tissues. As expected, these results also show that detecting tumor in homogeneous fatty breast tissue is easier than in quasi-heterogeneous and homogeneous fibro-glandular tissues, respectively.

Normalized imaging results of breast cancer tumor with 2 mm diameter are presented in logarithmic scale, as shown in Fig. 9. Normalization is done within each breast phantom case, separately. Comparing the calculated signal energies of the conformal bow-tie antenna with the planar bow-tie antenna, signal levels increase when spherical conformal antennas are used. The increment is 4.8 dB, 6.9 dB, and 3.1 dB in the presence of homogeneous fatty breast, quasi-heterogeneous, and homogeneous fibro-glandular breast phantoms, respectively.

On the other hand, the 50 cm \times 40 cm imaging area in Fig. 7 is sampled with 1-mm pixel resolution and the DAS algorithm was performed on a single core of an Intel i5-2410M @ 2.30 GHz. In this case, the computation time is too long (i.e., more than half of a day) to obtain only one 2-D microwave image. Therefore, parallel computing tools on graphics processing units of a workstation with multicores as well as computationally efficient algorithms should be used to speed up the computation time for imaging [29].

The calibration measurements over the breast without tumor (equation (2)) cannot be used in clinic applications. Because differential imaging method [6] does not require a background measurement, it can be used in clinical scenarios. The first measurement should be performed with the array in a given position, then the array is rotated (in a horizontal plane, around its central vertical axis) and a second measurement is recorded. Those two measurements are then subtracted, resulting in a differential signal, which is used as an input into imaging algorithm. A

detailed description of this method can be found in [6]. More anatomically realistic breast phantom models with dispersive dielectric properties [27-28] should be included to observe the feasibility of the spherical conformal bow-tie antennas better for use in the microwave imaging system. However, obtained results are encouraging that an improvement could be also achieved by adding more and smaller conformal antennas to the array encircling the breast, to enhance detection capability of the microwave imaging system more [6].

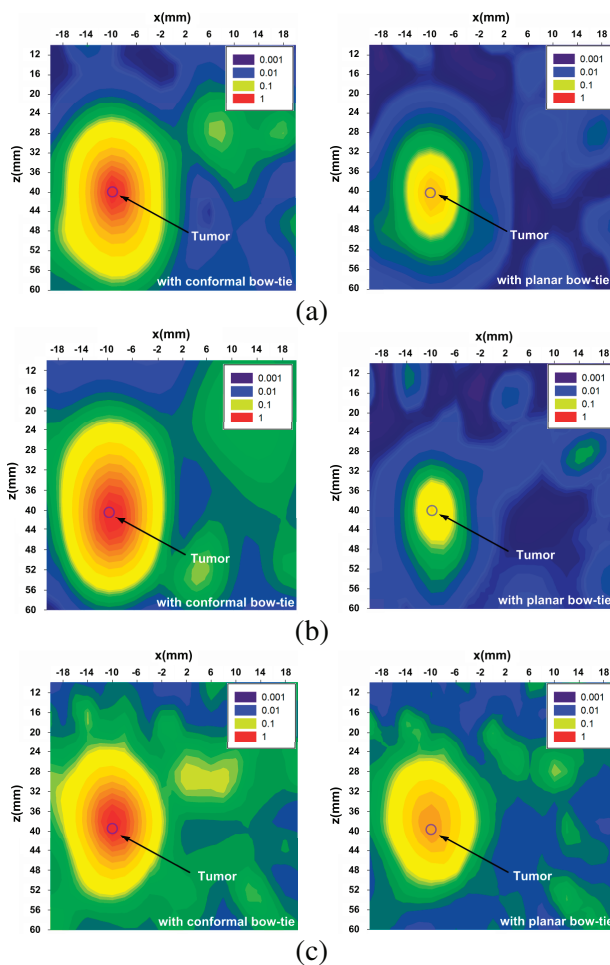


Fig. 9. Images of breast cancer tumor with 2 mm diameter embedded in (a) homogeneous fatty breast, (b) quasi-heterogeneous, and (c) homogeneous fibro-glandular breast phantoms.

IV. CONCLUSION

An UWB spherical conformal bow-tie antenna array surrounding the breast has been designed

and tested on the full-wave electromagnetic simulator, in order to investigate the effects of conformal structure on tumor detection capability of the microwave radar-based imaging system. The proposed bow-tie antenna with spherical curvature would be an attractive candidate element for radar-based breast cancer detection to achieve good polarization matching with spherical waves inside the breast as well as low pulse distortion and low mutual effects between array elements.

Time domain behavior of the conformal antenna has indicated better pulse distortion performance through the breast, comparing with the planar bow-tie. The mutual coupling effects of the conformal antenna have been reduced in overall compared to that of the planar antenna, too. Images of the spherical tumor with 2 mm diameter have been successfully formed by using the DAS algorithm. Tumor responses have been increased in between 2.3 dB and 5.7 dB with the use of the spherical conformal antenna. Obtained simulation results are reasonably reliable and promising; however, experimental work based on microwave radar-based differential imaging technique is required with anatomically realistic breast phantom models.

REFERENCES

- [1] S. Iudicello and F. Bardati, "Functional imaging of compressed breast by microwave radiometry," *Applied Computational Electromagnetics Society (ACES) Journal*, vol. 24, no.1, pp. 64-71, 2009.
- [2] L. Wang, X. Zhao, H. Sun, and G. Ku, "Microwave-induced acoustic imaging for biological tissues," *Rev. Sci. Instrum.*, vol. 70, no. 9, pp. 3744-3748, 1999.
- [3] A. Bulyshev, S. Semenov, A. Souvorov, R. Svenson, A. Nazarov, Y. Sizov, and G. Tatsis "Computational modelling of three-dimensional microwave tomography of breast cancer," *IEEE Trans. Biomed. Eng.*, vol. 48, no. 9, pp. 1053-1056, 2001.
- [4] E. Fear, X. Li, S. Hagness, and M. Stuchly, "Confocal microwave imaging for breast tumor detection: Localization in three dimensions," *IEEE Trans. Antennas Propag.*, vol. 49, no. 8, pp. 812-822, 2002.
- [5] E. J. Bond, X. Li, S. C. Hagness, and B. D. Van Veen, "Microwave imaging via space-time beamforming for early detection of breast cancer," *IEEE Trans. Antennas Propag.*, vol. 51, no.8, pp. 1690-1705, 2003.

- [6] M. Klemm, J. Leendertz, D. Gibbins, I. Craddock, A. Preece, and R. Benjamin, "Microwave radar-based differential breast cancer imaging: Imaging in homogeneous breast phantoms and low contrast scenarios," *IEEE Trans. Antennas Propag.*, vol. 58, pp. 2337-2344, 2010.
- [7] X. Li, S. Davis, S. Hagness, D. Van der Weide, and B. Van Veen, "Microwave imaging via space-time beamforming: Experimental investigation of tumor detection in multilayer breast phantoms," *IEEE Trans. Microw. Theory Tech.*, vol. 52, no. 8, pp. 1856-1865, 2004.
- [8] S. Hagness, A. Taflove, and J. Bridges, "Wideband ultralow reverberation antenna for biological sensing," *Electronics Letters*, vol. 33, no. 19, pp. 1594-1595, 1997.
- [9] X. Yun, E. Fear, and R. Johnston, "Compact antenna for radar-based breast cancer detection," *IEEE Trans. Antennas Propag.*, vol. 53, no. 8, pp. 2374-2380, 2005.
- [10] H. Kanj and M. Popovic, "Two-element T-array for cross-polarized breast tumor detection," *Applied Computational Electromagnetics Society (ACES) Journal*, vol. 23, no. 3, pp. 249-254, 2008.
- [11] N. Tavassolian, S. Nikolaou, and M. Tentzeris, "A flexible UWB elliptical slot antenna with a tuning uneven U-shape stub on LCP for microwave tumor detection," *Asia-Pacific Microwave Conference*, Bangkok, Thailand, pp. 1-4, Dec. 2007.
- [12] D. Gibbins, M. Klemm, I. Craddock, J. Leendertz, A. Preece, and R. Benjamin, "A comparison of a wide-slot and a stacked patch antenna for the purpose of breast cancer detection," *IEEE Trans. Antennas Propag.*, vol. 58, no. 3, pp. 665-674, 2010.
- [13] J. Bourqui, M. Okoniewski, and E. Fear, "Balanced antipodal vivaldi antenna for breast cancer detection," *The Second European Conference on Antennas and Propagation*, Edinburgh, UK, pp. 1-5, Nov. 2007.
- [14] İ. Ünal, B. Türetken, K. Sürmeli, and C. Canbay, "An experimental microwave imaging system for breast tumor detection on layered phantom model," *URSI GASS 2011*, İstanbul, Turkey, pp. 1-4, Aug. 2011.
- [15] B. Mohammed, A. Abbosh, and M. Bialkowski, "Design of tapered slot antenna operating in coupling liquid for ultrawideband microwave imaging systems," *APSURSI*, Washington, USA, pp. 145-148, July 2011.
- [16] Z. Šipuš, S. Škokić, and N. Burum, "Performance analysis of spherical stacked-patch antennas," *18th Int. Conference on Applied Electromagnetics and Communications*, Dubrovnik, Croatia, pp. 1-4, Oct. 2005.
- [17] R. Conceição, M. O'Halloran, M. Glavin, and E. Jones, "Comparison of planar and circular antenna configurations for breast cancer detection using microwave imaging," *Progress In Electromagnetics Research*, PIER 99, pp. 1-20, 2009.
- [18] X. Yun, R. Johnston, and E. Fear, "Radar-based microwave imaging for breast cancer detection: Tumor sensing with cross-polarized reflections," *Antennas and Propagation Society Int. Symposium*, California, USA, pp. 2432-2435, June 2004.
- [19] J. Stang, W. Joines, Q. Liu, G. Ybarra, R. George, M. Yuan, and I. Leonhardt, "A tapered microstrip patch antenna array for use in breast cancer screening via 3D active microwave imaging," *Antennas and Propagation Society Int. Symposium*, Charleston, SC, USA, pp. 1-4, June 2009.
- [20] İ. Ünal, B. Türetken, U. Buluş, and C. Canbay, "Analysis of the electromagnetic field scattered by a spherical breast tumour model," *URSI-EMTS 2013*, Hiroshima, Japan, pp. 574-577, May 2013.
- [21] İ. Ünal, *A New Ultrawide-Band (UWB) Microwave Imaging System with Minimized Mutual Coupling Effects for Breast Tumor Detection*, Ph.D. Thesis, Yeditepe University, Department of Electrical and Electronics Engineering, İstanbul, Turkey, March 2013.
- [22] N. Tavassolian, H. Kanj, and M. Popović, "The effect of breast glands on microwave tumor sensing with "Dark Eyes" antenna," *Antennas and Propagation Society Int. Symposium*, Albuquerque, NM, USA, pp. 291-294, July 2006.
- [23] İ. Ünal, B. Türetken, U. Buluş, and C. Canbay, "Analysis of dispersive effects of breast phantom model on ultra wideband microwave imaging of breast cancer tumor," *IASTED International Conference on Biomedical Engineering*, Innsbruck, Austria, pp. 1-6, Feb. 2013.
- [24] C. Canbay, *Antennas and Propagation I*, Yeditepe University Press, İstanbul, 1997.
- [25] A. Abbosh and M. Bialkowski, "Compact directional antenna for ultra wideband microwave imaging systems," *Antennas and Propagation Society Int. Symposium*, Charleston, SC, USA, pp. 1-4, June 2009.
- [26] Rohde & Schwarz GmbH & Co. KG, ZNB 8 Vector Network Analyzer, Product Data Sheet.
- [27] M. Lazebnik, M. Okoniewski, J. Booske, and S. Hagness, "Highly accurate debye models for normal and malignant breast tissue dielectric properties at microwave frequencies," *IEEE Microwave and Wireless Components Letters*, vol. 17, no. 12, pp. 822-824, 2007.
- [28] D. Winters, J. Shea, P. Kosmas, B. Van Veen, and S. Hagness, "Three-dimensional microwave breast imaging: Dispersive dielectric properties

estimation using patient-specific basis functions,” *IEEE Trans. Medical Imag.*, vol. 28, no. 7, pp. 969-981, 2009.

- [29] A. Capozzoli, C. Curcio, A. Di Vico, and A. Liseno, “NUFFT- & GPU-based fast imaging of vegetation,” *IEICE Trans. Commun.*, vol. E94-B, no. 7, pp. 2092-2103, 2011.



İlhami Ünal received his B.Sc., M.Sc., and Ph.D. degrees from Yeditepe University, Istanbul, Turkey in 2002, 2005 and 2013, respectively, in Electrical and Electronics Engineering. Since Sept. 2013, he has been working as a chief senior researcher at Millimeter and Terahertz Technologies Research Laboratories (MILTAL) at the Material Institute of TUBITAK-MRC. His research interests include antennas and propagation, scattering of electromagnetic fields, microwave imaging and bioelectromagnetics. He is also the Associate Editor of the Turkish Journal of Electrical & Computer Sciences.



Bahattin Türetken has received M.Sc. and Ph.D. degrees from Istanbul Technical University, Istanbul, Turkey in 1998 and 2002, respectively. He received Associate Professor title in 2008. He has been working as chief researcher at TUBITAK-UEKAE (National Research Institute of Electronics and Cryptology) EMC & TEMPEST Test Center. He managed Electromagnetic and Research Group (EMARG) and the project of Antenna Test and Research Center between 2009 and 2012. He has been the director of “Millimeter and Terahertz Technologies Research Laboratories (MILTAL)” since 2012. He was awarded “Young Scientist Award” by URSI in 1999 and “Young Scientist Paper” by MMET in 2000. His research topics are radar, antenna design and testing, computational electromagnetic, diffraction & scattering EM Problems, civilian and military EMC/EMI problems, terahertz applications, radiometry, biomedical Imaging, implant devices.



Cahit Canbay received the B.Sc. degree from Physics Department of Istanbul University, Turkey. He received his Ph.D. degree in Electronics and Communications Engineering from Yıldız Technical University, Turkey. His research interests include electromagnetic fields, antennas and propagation, biological effects of electromagnetic fields on human health, optical fiber systems and their problems, optoelectronics, smart antennas and propagation for wireless systems, numerical methods in electromagnetic problems and electromagnetic compatibility.